Proceedings of the 13th
IEEE International Conference on Nanotechnology
Beijing, China, August 5-8, 2013

A High-Throughput and Low-Cost 3D Imaging System for Flowing Escherichia Coli

Tak Kit Lau, Yun-hui Liu, *Fellow, IEEE*, Yu-jie Lu, Chi-ming Cheuk, Kai-wun Lin

***Abstract*— In this paper, we present a novel design of low-cost, high-throughput hologram-based 3D imaging system towards the development of a detection system for Escherichia coli (E. coli). This focusing-free system can image food samples flowing in a transparent microchannel under illumination of RGB lasers through a pinhole, and yields their 3D structures in real-time using hologram-based reconstruction algorithms. We solve two key technical problems in order to realize the system: 1) implementation of a high-speed (200fps) imaging system for capturing full-frame holograms of cells flowing in microchannels; 2) reconstruction of 3D structure of E. coli by characterizing the holograms under low-cost incoherent light sources such as the incoherent laser diodes. Market-dominating food pathogen detection systems using the polymerase chain reaction (PCR) are very slow (10-20 hours/ml) in addition to their high costs. Moreover, they cannot detect the viable but non-culturable (VBNC) E. coli, which orchestrated the recent massive and deadly food poisoning outbreaks in Europe and North America. The estimated cost of the proposed system is less than US$11,000 and its speed is over 1,000 times faster than the existing methods.**

I. Introduction

E. coli has been a key indicator for fecal contamination in food [1], [2]. Modern detection methods like the real-time polymerase chain reaction (PCR) [3], [4], [5] and the nucleic acid sequence based amplification (NASBA) [8,9] can detect E. coli but they take 10 to 20 hours for results and cost more than a million Hong Kong Dollars. Worse still, a massive food poisoning outbreak in Germany and North America revealed that, the existing E. coli detection methods are worthless in finding the virulent serogroups of viable-but-non-culturable (VBNC) E. coli [6], [7], [8], [9]. As a result, a low-cost and high-throughput detection system for E. coli and VBNC E. coli is desperately needed worldwide.

In this paper, we present our works in developing a low-cost and high-throughput 3D imaging system for detection of E. coli, including the hard-to-detect VBNC E. coli. The fundamental working principle is similar to the digital holographic microscopes (DHMs) in the market, which employ Gabor's hologram theory [10] for reconstruction of sample's 3D structure. However, our design, methodology and functionality are totally different. The proposed system leverages low-cost, incoherent, red, green and blue laser diodes as light sources, and yields the sample's 3D structure with chromatic features in real-time. In addition, the imaging component in the system comprises a high-end scientific CMOS and a field-programmable gate array (FPGA) for a stable image acquisition and processing. These configurations and functionalities facilitate an innovative E. coli detection system with a cost of US$11,000 and a detection 1,000 times faster than the existing products in the market.

Modern detection methods for E. coli include the immunoassay methods [11], the real-time polymerase chain reaction (real-time PCR) [3] and the nucleic acid sequence based amplification (NASBA) [4], [12]. The immumoassay methods normally take 4 to 7 days. Real-time PCR and NASBA are genetic amplification methods and now at front-line of food pathogen detection worldwide to detect a wide range of virulent microorganisms. The genetic amplification methods involve several key steps like samples enrichment, denaturation, annealing and extension. NASBA does not require a precise and hierarchical thermal control as found in the real-time PCR. Nonetheless, both methods require a long sample preparation time including the process ofcell culturing. A recent development in the immunomagnetic separation (IMS) [2], [13], [14], [15] can speed up the overall detection time, but the real-time PCR and NASBA are still sensitive to inhibitors and require extensive sample preparation in addition to their extremely high cost. A cell-phone based E. coli detection method has recently been proposed and evaluated [16], [17], [18]. Their method relies on dying fluorescent particles [19], particularly the streptavidin conjugated quantum dots, along with the biotinylated anti-E. coli antibodies and other antibodies for capture and detection, on E. coli for the detection. After incubation and sample preparation, they use the camera in a cell-phone to look for the fluorescent spots in the dyed samples. The overall detection time takes 4-5 hours. The immunoassay method is recently re-visited and showed promises of fast E. coli detection in less than an hour [20]. However, it requires a rather high concentration of nearly 50 CFUs per milli-liter of E. coli in samples for detection.

In this paper, we address three key challenges that pertain to the development of the proposed system. 1) We characterize the hologram under incoherent light sources to rectify the undesired fringes that obscures the reconstruction of 3D structures of E. coli. 2) We develop a method to combine three holograms, that are illuminated by red, green and blue lasers respectively, then yield 3D chromatic structures of the samples in real-time. 3) We implement a high-speed (200fps) imaging system for capturing the full-frame holograms.

From a technology perspective, we adapt the hologram-based reconstruction algorithms developed in Fourier optics [21], specifically the Fresnel-Kirchhoff diffraction integral and the Rayleigh-Sommerfeld integral [22], with a

All authors are with the Department of Mechanical and Automation Engineering, The Chinese University of Hong Kong, China. E-mail: {tklau,yhliu}@mae.cuhk.edu.hk

978-1-4799-0676-5/13/$31.00 ©2013 IEEE

series of image processing techniques to synthesize 3D chromatic images of the microorganism in food samples. The technology of color hologram generation is widely adapted in the fields of picture coding and printing industry [23], but it is not further developed to accommodate in the holographic microscopy or the reconstruction of hologram.

The paper is arranged as follows: Section II explains the principle of holography, and Section II-B details methods for the reconstruction of holograms. Section II-C includes the reconstruction method with objective lens. Section II-D discusses the algorithms for the generation of depth maps. Section III gives and analyzes the experimental results. Finally, Section IV closes with a conclusion.

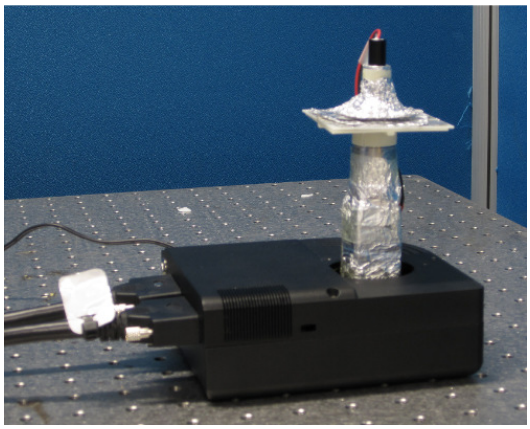

Fig. 1. A prototype of our high-throughput, low-cost 3D imaging system for the detection of E. coli. Only one laser diode is incorporated in this configuration. The imaging system foundation originates from Pho Imaging's Oria imaging system (#ORIA-2-CL-C-S), and is modified to fit our application.

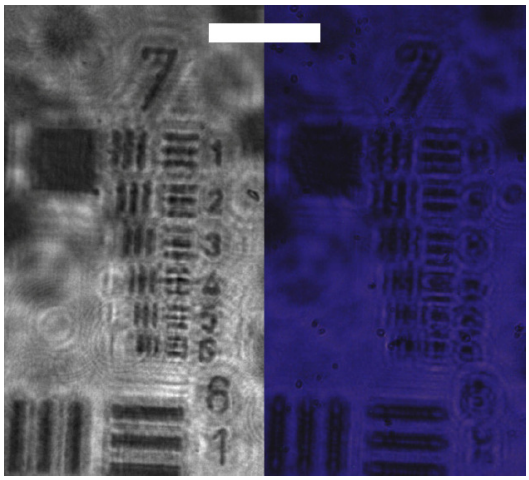

Fig. 2. (Left) A reconstructed hologram; (Right) The original hologram of a USAF test object captured by our system. The lenght of white bar is of 50μm.

II. Reconstruction Algorithm

A. A Brief Review of Holography

Microscope holography is first introduced by Gabor in 1948 [24], which at first was used to avoid spherical aberrations of electron lenses. The whole recording system includes a point source, an object and a photographic plane. The primary wave emitted from the point source (namely the reference wave), and the secondary wave scattered by the object (namely the object wave) interfere together at the holographic plane, and create an intensity recording - the hologram. Over the years, this holography principle received enormous attention in optical microscopy as the 3D information of the object can be, in principle, retrieved by a single image of the object's hologram.

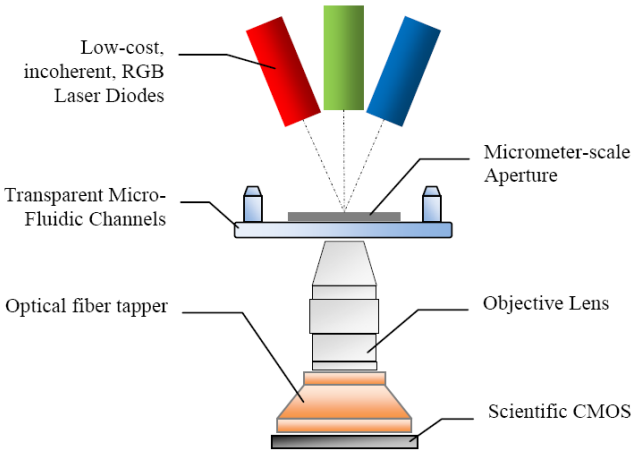

Fig. 3. Schematics of our system.

The holography principle, however, suffered from an inherent noise coined as the twin image problem. Many aimed at eliminating this noise and in 1962, Leith and Upatnieks [25] addressed the twin image by proposing an off-axis setup to spatially separates the twin image. Other methods like Phase Shifting Holography [26], [27] are also proposed to solve this problem by altering the phase of the reference wave and reconstructing using multiple holograms.

In the late 1960s and early 1970s, the digital holography (DH) [28], [29], [30] appeared and replaced the photographic plane with a digital sensor and the reconstruction is carried out on computers. However, the computers and sensors were incompetent to perform reconstruction in real time. Under the fast-paced development of the computation capacity and the booming digital imaging resolution, DH revived in 1990s and was advanced to numerically suppress the twin image problem using various algorithms. Currently, the modern DH method is a low-cost and focus-free approach to record, reconstruct and observe the 3D information of an object.

B. Inline Digital Hologram

Figure 4 illustrates the basic setup of Gabor's inline holography [24]. In general, the numerical reconstruction method of this setup can be divided into two types. The first one is based on the Kirchoff-Helmholtz transform [31], [32], [33]. The second one is based on the Fresnel-Kirchhoff intergral [34], [35], [36]. Here, we adapt the latter approach and analyze Gabor's inline holography using an operator

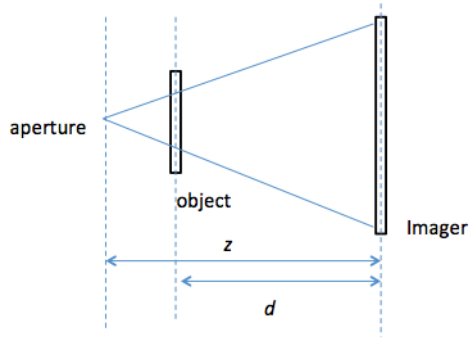

Fig. 4. Schematic of Gabor inline holography

provided by Goodman [21]. For the simplicity of this paper, we only consider 1-D case in the following analysis. The reader should note that this operator approach is based on the paraxial approximation, and omits most of the constant coefficients (e.g. The spherical wave is described as $e^{j\frac{k}{2z}x^2}$ instead of $\frac{1}{r}e^{jkr}$, where k is also the wave number, z is the distance between the point source and the plane and $r=\sqrt{x^2+z^2}$). To demonstrate the whole process, we first briefly introduce the operators needed in this approach.

The definition of the operator Q is

$$Q[c]\{U(x)\} = e^{j\frac{k}{2}cx^2}U(x) \tag{1}$$

where $k=2\pi/\lambda$ and c is an inverse length.

The definition of the operator V is

$$V[b]\{U(x)\} = b^{1/2}U(bx) \tag{2}$$

where b is dimensionless.

The definition of the operator R is

$$R[d]\{U(x_1)\} = \frac{1}{\sqrt{j\lambda d}}\int_{-\infty}^{\infty} U(x_1)e^{j\frac{k}{2d}(x_2-x_1)^2}dx_1 \tag{3}$$

where d is the distance of propagation and x_2 is the coordinate that applies after propagation.

Optical lenses can be represented by the operator Q which changes the phase of the incident light. We can also convert between the plane wave and the spherical wave using operator Q. Operator V is a simple scaling operator while Operator R represents free space propagation which can be seen as an approximation of the Huygens-Fresnel principle. With these operators above we can formulate the recording process of the holograms as follows. Let P be the operator of this system, we have,

$$P = R[d]Q[\frac{1}{z-d}] \tag{4}$$

The object is illuminated by a point source that is $(z-d)$ away from the object. Then, the light propagates over the distance of d before it was imaged by a digital imager. We can rewrite (4) into (5) and (6) using the relationships between different operators as shown in [21],

$$P = Q[\frac{1}{z}]R[\frac{z}{z-d}d]V[\frac{z-d}{z}] \tag{5}$$

$$P = Q[\frac{1}{z}]V[\frac{z-d}{z}]R[\frac{z-d}{z}d] \tag{6}$$

We can design an inverse system P^{-1} based on any of the three expressions of the operators. In principle, we can fully reconstruct an object on object plane from a hologram using any of the inverse systems designed below if the amplitude and phase information are given at the imager's plane. However, an imager generally can only record the amplitude information of the light field. Without special setup like the off-axis holography, we assume that the wave field at the imager's plane is a plane wave or a spherical wave when the amplitude of the object wave is much smaller than the reference wave.

a) Method 1 - Reconstruction using (4): From (4), we can reverse the hologram recording process and have,

$$P^{-1} = Q[-\frac{1}{z-d}]R[-d] \tag{7}$$

Due to the loss of the phase information, the hologram cannot be reconstructed using (7), unless we apply a Q operator at the beginning and convert the recorded hologram into a light field of ideal spherical wave. Therefore, (7) is rewritten to a more practical representation,

$$P^{-1} = Q[-\frac{1}{z-d}]R[-d]Q[\frac{1}{z}] \tag{8}$$

b) Method 2 - Reconstruction using (5): If we denote the transmittance of the object as $O(x)$, we can derive the light field on the imager's plane by applying the system operator P. Then the recorded hologram can be described by, (9).

$$\begin{aligned} H(x) &= |P\{O(x)\}| \\ &= |Q[\frac{1}{z}]R[\frac{z}{z-d}d]V[\frac{z-d}{z}]\{O(x)\}| \\ &= |R[\frac{z}{z-d}d]V[\frac{z-d}{z}]\{O(x)\}| \end{aligned} \tag{9}$$

The light is propagating as a plane wave, so we can directly backpropagate over the distance of $\frac{z}{z-d}d$ and a magnified object image as shown in (10) can be obtained,

$$\begin{aligned} R[-\frac{z}{z-d}d]\{H(x)\} &\approx R[-\frac{z}{z-d}d]R[\frac{z}{z-d}d]V[\frac{z-d}{z}]\{O(x)\} \\ &= V[\frac{z-d}{z}]\{O(x)\} \end{aligned} \tag{10}$$

Therefore, we can have

$$P^{-1} = R[-\frac{z}{z-d}d] \tag{11}$$

c) Method 3 - Reconstruction using (6): The reconstruction steps based on (6) is similar to the Method 2 except that before performing the back propagation, the holograms must be virtually magnified by setting the pixel size of the imager $\frac{z-d}{z}$ times smaller than its original dimension.

Comparing the three reconstruction methods above, the Method 2 requires the least computation effort and generates a magnified object image which can help in inspecting small objects like the E. coli. Therefore we adapt this approach to reconstruct the 2-D image of the hologram.

C. 2-D Reconstruction with Objective Lens

To further amplify the object, our system is equipped with an objective lens and is placed between the object and the imager. Figure (5) illustrates the design of this setup. The

objective is not to form the image right at the plane of the imager which is a necessary condition of the traditional image recording system. On the contrary, the image of the object can be reconstructed from image taken at any location on the side of the imager's plane, provided that the intensity of image can be sufficiently imaged by the imager, using numerical reconstruction methods as described in the previous section. We can also formulate this process using

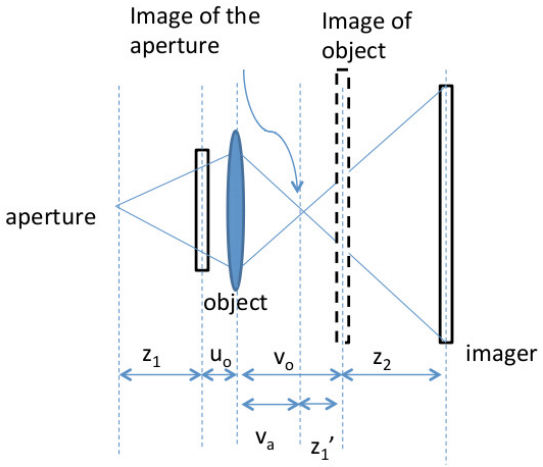

Fig. 5. Schematic of our system

the operators as described in Section II-B. As we can see from Fig. 5, the object is first illuminated by a spherical wave, and after propagating over the distance of u_0, the light illuminates at the objective and then propagates again over the distance of $z_2 + v_0$. Denoting P as the system operator, we have,

$$P = R[z_2]R[v_0]Q[-\frac{1}{f}]R[u_0]Q[\frac{1}{z_1}], \tag{12}$$

Immediately,

$$P^{-1} = R[\frac{z_2 + z_1^{'}}{z_1^{'}} z_2] \tag{13}$$

and the total magnification factor of the system can be written as,

$$\beta = \beta_1 * \beta_2 \tag{14}$$

where β_1 is the magnification factor of the objective, and $\beta_2 = \frac{z_1^{'}+z_2}{z_1^{'}}$.

D. Depth map generation

Although a hologram embeds the 3-D information of the imaged object, the reconstruction of 3-D geometry of the object is not trivial. Many used the difference of the reconstructed phase as an indicator [37], [38] to perform 3-D reconstruction. However, it requires the phase information at the object plane. As inline holography cannot provide phase information, we adapt a method proposed by McElhinney [39] to perform the generation of depth map of the imaged samples. The procedure is given below: (1) Reconstruct images from the holograms at different depths using the 2-D reconstruction method; (2) Determine a kernel to calculate the focus depth of each pixel; (3) Evaluate the results that are generated using different depth parameters and find the depths with the sharpest features in the images; (4) Combine the depth information of each pixel in the image and generate the depth map.

There are two critical issues in this procedure. The first one is the calculation of focus depth in the kernel. Elhinney made use of the variance as an indicator, and others used the normalized cross correlation [40]. We adapt the variance in the kernel as an indicator to determine the focus depth, i.e. L_2 norm divided by L_1 norm of the pixel in the window. [41] proved that the sum of L_2 norm of the whole hologram remains as constants after performing reconstruction at different depths. And the sum of L_1 norm of the whole hologram can be used as a criterion to estimate the focus depth of the whole image. After the focus depth is determine, another critical parameter is the window size in the kernel. Obviously, the larger the window size the more accurate results at the cost of loss of image resolution. On the contrary, the smaller the window size the higher image resolution preserved but at a cost of higher image noise. To achieve a balanced performance, we combine the results using large and small window sizes by keeping the mutually similar results in the image. The procedures of this method is given in Fig (7).

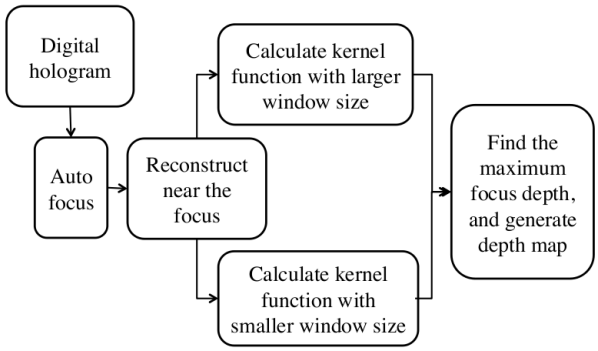

Fig. 6. Basic steps of the generation of depth map

III. Experimental Results

Using our setup as shown in Fig. 1, holograms (Fig. 2) are captured under illumination of an incoherent ultraviolet laser (i.e. $\lambda = 395.2nm, \pm 10nm$). The imaging system is extended from an imaging system from Pho Imaging[1], which features a pixel array of 2048*2048 with 12-bit color depth and a dynamic range of 90dB. Another set of holograms are taken by another setup based on Gabor's inline hologram. The results are given in Fig. 7. The test object is the USAF 1951 positive slide glass.

In Fig. 7, we as well exhibits the reconstruction results using different reconstruction methods based on Gabor's inline holography as explained in Section II-B. The first

[1]http://www.pho-imaging.com

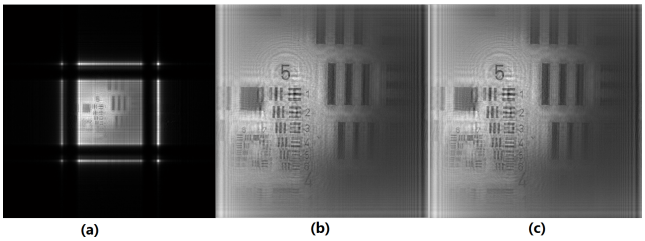

Fig. 7. Reconstruction results using Gabor's inline holography (a) By (4); (b) By (5); (c) By (6)

.

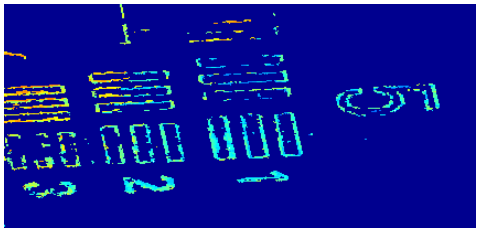

Fig. 8. Results of depth map generation

.

method yields a reconstructed image of the testing object using the original image size while the other two methods yield magnified images. Figure 2 exhibits the results by our system with a 40x oil immersion objective lens. We can observe the Group 6 and 7 which is the smallest group of our testing target. The shortest length width among these two groups is about 2.19um. The computation time is less than 20ms for the reconstruction of a single, full-size hologram. The results of the depth map is given in Fig. 8. The resolution can be improved by replacing the objective lens with a higher magnification one. The results demonstrate that the proposed system can image micro-object with a resolution of about 2um and is expected to achieve a resolution of 0.8um when using a 100x objective lens. As the size of E. coli is around 1 to 3um, the system is capable of capturing of these samples with distinguishable resolution. We will further develop the system, particularly on the processing and classification of imaged samples using their chromatic and geometric features in complex food samples.

IV. Conclusion

The viable but non-culturable (VBNC) E. coli is fatal to human and is undetectable using the existing detection systems in food industry. The proposed focusing-free 3D imaging system can detect micro-object as small as 1 to 2um with a throughput of 40 minutes per ml, and hence can be further developed then deployed to detect the virulent strains of pathogenic E. coli at a speed that can be 1,000 times faster than today's top-notched E. coli detection products. At the core of our system is a high-speed, large field-of-view imaging system and a novel design of chromatic laser illumination setup. By leveraging holographic principles, we adapt Gabor's algorithm to yield 3D structures of the flowing E. coli in a micro-channel, and lay a promising foundation for the development of high-throughput, low-cost detection systems for E. coli in food samples.

Acknowledgment

The first author would like to give a warm thanks to Pho Imaging for providing the Oria imaging systems to facilitate the development of E. coli detection system, and to Prof. Andrew M. Chan from the Chinese University of Hong Kong for the E. coli samples.

References

[1] H. Hussein and T. Sakuma, "Prevalence of shiga toxin-producing escherichia coli in dairy cattle and their products," *Journal of Dairy Science*, vol. 88, no. 2, pp. 450–465, 2005.

[2] J. Lee and R. A. Deininger, "Detection of e. coli in beach water within 1 hour using immunomagnetic separation and atp bioluminescence," *Luminescence*, vol. 19, no. 1, pp. 31–36, 2004.

[3] N. Y. Fortin, A. Mulchandani, and W. Chen, "Use of real-time polymerase chain reaction and molecular beacons for the detection of escherichia coli o157: H7," *Analytical biochemistry*, vol. 289, no. 2, pp. 281–288, 2001.

[4] L. Heijnen and G. Medema, "Quantitative detection of e. coli, e. coli o157 and other shiga toxin producing e. coli in water samples using a culture method combined with real-time pcr," *J Water Health*, vol. 4, pp. 487–498, 2006.

[5] J. Holland, L. Louie, A. Simor, and M. Louie, "Pcr detection of escherichia coli o157: H7 directly from stools: evaluation of commercial extraction methods for purifying fecal dna," *Journal of clinical microbiology*, vol. 38, no. 11, pp. 4108–4113, 2000.

[6] L.-D. Dinu and S. Bach, "Detection of viable but non-culturable escherichia coli o157: H7 from vegetable samples using quantitative pcr with propidium monoazide and immunological assays," *Food Control*, 2012.

[7] R. Reissbrodt, I. Rienaecker, J. Romanova, P. Freestone, R. Haigh, M. Lyte, H. Tschäpe, and P. Williams, "Resuscitation of salmonella enterica serovar typhimurium and enterohemorrhagic escherichia coli from the viable but nonculturable state by heat-stable enterobacterial autoinducer," *Applied and environmental microbiology*, vol. 68, no. 10, pp. 4788–4794, 2002.

[8] L.-D. Dinu and S. Bach, "Induction of viable but nonculturable escherichia coli o157: H7 in the phyllosphere of lettuce: a food safety risk factor," *Applied and environmental microbiology*, vol. 77, no. 23, pp. 8295–8302, 2011.

[9] P. Aurass, R. Prager, and A. Flieger, "Ehec/eaec o104: H4 strain linked with the 2011 german outbreak of haemolytic uremic syndrome enters into the viable but non-culturable state in response to various stresses and resuscitates upon stress relief," *Environmental microbiology*, vol. 13, no. 12, pp. 3139–3148, 2011.

[10] D. Gabor, "Associative holographic memories," *IBM Journal of Research and Development*, vol. 13, no. 2, pp. 156–159, 1969.

[11] P. Evans, "Design of e. coli o157:h7 sampling and testing programs by industry," *FSIS Office of Public Health Science*, 2011.

[12] A. J. Baeumner, R. N. Cohen, V. Miksic, and J. Min, "Rna biosensor for the rapid detection of viable escherichia coli in drinking water," *Biosensors and Bioelectronics*, vol. 18, no. 4, pp. 405–413, 2003.

[13] F. Li, Q. Zhao, C. Wang, X. Lu, X.-F. Li, and X. C. Le, "Detection of escherichia coli o157: H7 using gold nanoparticle labeling and inductively coupled plasma mass spectrometry," *Analytical chemistry*, vol. 82, no. 8, pp. 3399–3403, 2010.

[14] S. Z. Hossain, C. Ozimok, C. Sicard, S. D. Aguirre, M. M. Ali, Y. Li, and J. D. Brennan, "Multiplexed paper test strip for quantitative bacterial detection," *Analytical and bioanalytical chemistry*, vol. 403, no. 6, pp. 1567–1576, 2012.

[15] B. H. Pyle, S. C. Broadaway, and G. A. McFeters, "Sensitive detection of escherichia colio157: H7 in food and water by immunomagnetic separation and solid-phase laser cytometry," *Applied and Environmental Microbiology*, vol. 65, no. 5, pp. 1966–1972, 1999.

[16] M. Lee, O. Yaglidere, and A. Ozcan, "Field-portable reflection and transmission microscopy based on lensless holography," *Biomedical optics express*, vol. 2, no. 9, p. 2721, 2011.

[17] H. Zhu, O. Yaglidere, T.-W. Su, D. Tseng, and A. Ozcan, "Cost-effective and compact wide-field fluorescent imaging on a cell-phone," *Lab on a Chip*, vol. 11, no. 2, pp. 315–322, 2011.

[18] H. Zhu, U. Sikora, and A. Ozcan, "Quantum dot enabled detection of escherichia coli using a cell-phone," *Analyst*, vol. 137, no. 11, pp. 2541–2544, 2012.

[19] M. Oda, M. Morita, H. Unno, and Y. Tanji, "Rapid detection of escherichia coli o157: H7 by using green fluorescent protein-labeled pp01 bacteriophage," *Applied and environmental microbiology*, vol. 70, no. 1, pp. 527–534, 2004.

[20] S. Wang, F. Inci, T. L. Chaunzwa, A. Ramanujam, A. Vasudevan, S. Subramanian, A. C. F. Ip, B. Sridharan, U. A. Gurkan, and U. Demirci, "Portable microfluidic chip for detection of escherichia coli in produce and blood," *International journal of nanomedicine*, vol. 7, p. 2591, 2012.

[21] J. W. Goodman, *Introduction to Fourier optics*. Roberts & Company Publishers, 2005.

[22] T. Tommasi and B. Bianco, "Computer-generated holograms of tilted planes by a spatial frequency approach," *JOSA A*, vol. 10, no. 2, pp. 299–305, 1993.

[23] M. Kawabata, A. Sato, I. Sumiyoshi, and T. Kubota, "Photopolymer system and its application to a color hologram," *Applied optics*, vol. 33, no. 11, pp. 2152–2156, 1994.

[24] D. Gabor, "A new microscopic principle," *Nature*, vol. 161, no. 4098, pp. 777–778, 1948.

[25] E. Leith and J. Upatnieks, "Reconstructed wavefronts and communication theory," *Nature*, vol. 161, no. 4098, pp. 777–778, 1948.

[26] W. Zhou, Q. Xu, Y. Yu, and A. Asundi, "Phase-shifting in-line digital holography on a digital micro-mirror device," *Optics and Lasers in Engineering*, vol. 47, no. 9, pp. 896–901, 2009.

[27] I. Yamaguchi and T. Zhang, "Phase-shifting digital holography," *Optics letters*, vol. 22, no. 16, pp. 1268–1270, 1997.

[28] J. W. Goodman, "Digital image formation from electronically detected holograms," in *Computerized Imaging Techniques*. International Society for Optics and Photonics, 1967, pp. 176–181.

[29] T. S. Huang, "Digital holography," *Proceedings of the IEEE*, vol. 59, no. 9, pp. 1335–1346, 1971.

[30] M. Kronrod, N. Merzlyakov, and L. Yaroslavskii, "Reconstruction of a hologram with a computer," *Soviet Physics Technical Physics*, vol. 17, p. 333, 1972.

[31] J. Garcia-Sucerquia, W. Xu, S. K. Jericho, P. Klages, M. H. Jericho, and H. J. Kreuzer, "Digital in-line holographic microscopy," *Applied optics*, vol. 45, no. 5, pp. 836–850, 2006.

[32] W. Xu, M. Jericho, I. Meinertzhagen, and H. Kreuzer, "Digital in-line holography of microspheres," *Applied optics*, vol. 41, no. 25, pp. 5367–5375, 2002.

[33] ——, "Digital in-line holography for biological applications," *Proceedings of the National Academy of Sciences*, vol. 98, no. 20, pp. 11 301–11 305, 2001.

[34] J. P. Ryle, S. McDonnell, and J. T. Sheridan, "Lensless multispectral digital in-line holographic microscope," *Journal of Biomedical Optics*, vol. 16, no. 12, pp. 126 004–12 600 417, 2011.

[35] K. M. Molony, B. M. Hennelly, D. P. Kelly, and T. J. Naughton, "Reconstruction algorithms applied to in-line gabor digital holographic microscopy," *Optics Communications*, vol. 283, no. 6, pp. 903–909, 2010.

[36] S. Lai, B. Kemper, and G. von Bally, "Off-axis reconstruction of in-line holograms for twin-image elimination," *Optics communications*, vol. 169, no. 1, pp. 37–43, 1999.

[37] J. Min, B. Yao, P. Gao, R. Guo, B. Ma, J. Zheng, M. Lei, S. Yan, D. Dan, T. Duan *et al.*, "Dual-wavelength slightly off-axis digital holographic microscopy," *Applied optics*, vol. 51, no. 2, pp. 191–196, 2012.

[38] C. Depeursinge, T. Colomb, Y. Emery, J. Kuhn, F. Charriere, B. Rappaz, and P. Marquet, "Digital holographic microscopy applied to life sciences," in *Engineering in Medicine and Biology Society, 2007. EMBS 2007. 29th Annual International Conference of the IEEE*. IEEE, 2007, pp. 6243–6246.

[39] C. Mc Elhinney, B. Hennelly, J. McDonald, and T. Naughton, "Segmentation of macroscopic object digital holographic reconstructions using extracted depth information," in *Proc. of SPIE Vol*, vol. 7000, 2008, pp. 700 003–1.

[40] T. Pitkäaho and T. J. Naughton, "Calculating depth maps from digital holograms using stereo disparity," *Optics letters*, vol. 36, no. 11, pp. 2035–2037, 2011.

[41] F. Dubois, C. Schockaert, N. Callens, C. Yourassowsky *et al.*, "Focus plane detection criteria in digital holography microscopy by amplitude analysis," *Opt. Express*, vol. 14, no. 13, pp. 5895–5908, 2006.